International Journal for Housing Science and Its Applications
Publish August 6, 2025. Volume 46, Issue 3 Pages 8826-8839

https,//doi.org/10.70517/ijhsa463755

Optical Model of Mechanical Surface Inspection Based on Machine Vision

Yang Li[1,*], Wenzhuo Yang[1], Yongqi Wang[1], Chengjun Chen[1], Guangzheng Wang[1] and Xuefeng Zhang[1]
[1] School of Mechanical and Automotive Engineering, Qingdao University of Technology, Qingdao, Shandong, 266520, China
Corresponding authors: (e-mail: yuemingxingxi_1231@163.com).

Abstract In view of the influence of different illumination angles, color and intensity of light sources (LS) on the accuracy of crack detection, this text took rail surface detection (RSD for short here) as an example, constructed an optical model to describe the interaction process between light and surface, and realized the improvement of mechanical surface detection accuracy with the help of machine vision technology. Under the circumstances of different LS irradiation angle, LS color and LS intensity, the rail surface image was acquired by using the linear array CCD (charge coupled device) camera. In this text, Karpathy was used to divide the data set, preprocess the image, reduce image noise data and enhance image quality. In this text, gray co-occurrence matrix, Canny edge detection and color moment were used to extract rail surface features, and Convolutional Neural Network (CNN) model was used for feature detection. The results show that the difference between the gray-scale value (GSV) at the crack and the GSV of the normal rail is the largest at a light angle of 15°. Under the environment of white light irradiation and LS intensity of 5000 lumens, the detection accuracy of the CNN model was 98.3% when the illumination angle of the LS was 15°. The optical model of RSD using CNN can effectively improve the detection accuracy.

Index Terms Rail Surface, Defect Detection, Optical Model, Machine Vision, Convolutional Neural Network

I. Introduction

In modern industrial production, the quality of the mechanical surface is directly related to the performance and reliability of the product. It is very common for the mechanical surface to be uneven and burr, which would increase the physical friction between the machines. Under the action of long-term physical wear, the service life of the machinery would be reduced, the use of performance would be reduced, and even lead to the safety of the entire mechanical system. It is very important to inspect the mechanical surface and evaluate its quality. The traditional mechanical surface inspection method is manual visual inspection, which is judged by the operator with rich experience in the condition of suitable light by the naked eye. The disadvantages of traditional visual inspection methods are very obvious; the results of visual inspection are greatly affected by the subjective consciousness of the operator; the traditional visual mechanical surface inspection cost is too high; the efficiency is low, and the reliability of the detection results is not high. Machine vision has been widely applied to mechanical surface detection, and rapid and high-precision mechanical surface detection can be achieved through digital processing and analysis of mechanical surface images [1], [2]. In machine vision inspection, light is an extremely critical factor in the quality of an image. The optical model of mechanical surface inspection based on machine vision can analyze the inspection effect under different light conditions, so that the inspection of mechanical surface can be more automatic, accurate and efficient.

With the continuous development of industrial manufacturing, mechanical surface inspection plays a vital role in quality control. Many people use optical principles and image processing techniques to analyze the morphology, surface defects, smoothness and other parameters of mechanical surfaces. Xu Xiangyang combined ground-based laser scanning and laser tracking technology to improve high-precision surface modeling in deformation analysis. He verified and optimized spline approximation based on surface by using laser tracking corner cone reflectors. He used hypothesis testing to determine the maximum consistency of ground laser scanning and laser tracking in each period to select the best parameter settings and carry out accurate surface analysis of free-form surfaces [3]. Mei Shuang reconstructed image blocks on different Gaussian pyramid layers using convolutional de-noising automatic coding network and synthesized detection results from these different resolution channels to achieve surface detection and defect location, which can improve the robustness and accuracy of surface detection [4]. An unsupervised ML (machine learning) technique based on wavelet integrated alternating sparse dictionary matrix decomposition was proposed by Ahmed Junaid for the extraction of weaker

and deeper defect information in carbon fiber reinforced polymers using an optical pulsed thermal imaging system [5]. Sirca Jr Gene F used infrared spectrum to display differences in structural heat dissipation through thermal imaging cameras, and realizes defect detection of concrete structures [6]. Mechanical surface inspection optical models can be used to evaluate the quality of mechanical surface. These methods still have some shortcomings in dealing with complex surface defects, such as high false positive rate and insufficient detection accuracy.

Many researchers have explored the method of surface inspection using machine vision technology, and achieved certain results. Luo Qiwu analyzed the automatic visual detection of steel plate surface defects. With the continuous improvement of surface quality assurance requirements in flat steel industry, the machine vision classification of the extracted steel plate surface features can determine whether there are defects in the image and the type of defects, which can complete the complex defect detection task [7]. Baumgartl Hermann pointed out that it was a very complicated process to fabricate metal parts by laser-powder bed melting. He applied deep learning (DL) models to the defect detection in laser-powder bed fusion using in-situ temperature recording monitoring, which can identify defects such as layering and splashing with 96.80% accuracy [8]. Goh Guo Dong created and put into use a field monitoring system for extrude-based 3D printers that consists of a laptop that analyses the video stream and a camera attached to the print head [9]. A real-time rail surface defect detection approach based on machine vision was presented by Min Yongzhi, who also suggested optimizing rail surface flaws based on morphological analysis. By following the directional chain code, he discovered defect features. This approach realized the digital management of track problems since its maximum positioning time was 4.65 milliseconds and its maximum positioning failure rate was 5% [10]. The accuracy and robustness of the optical model of mechanical surface inspection using machine vision have certain dependence on lighting conditions, shooting angles, surface materials and other factors, and lack of analysis of mechanical surface inspection effects under different LS conditions.

The detection of surface flaws is a crucial step in ensuring the safety of railway transportation because railway track is a significant route of mass transportation. In this text, a linear array CCD camera is used to collect a large number of rail images and establish an optical system model. The Karpathy method is used to divide the data set, and the image is denoised and enhanced to improve the image quality and reduce the noise data. Texture features, defect features and shape features of rail surface images are extracted through gray co-occurrence matrix, Canny edge detection and color moment. In this text, CNN is used to detect rail surface features. In this text, different LS irradiation angles, different LS colors, and different LS intensity environments are set up. The results are as follows: (1) The greater the defect depth of the rail surface, the lower the GSV of the defect area. (2) The smaller the illumination angle of the LS, the lower the overall GSV of the rail surface image. (3) The difference between GSV of crack region and non-crack region under white light irradiation is more significant than that of red light and blue light under the same conditions. (4) Too high or too low LS intensity would lead to reduced accuracy of crack surface detection. (5) The effect of RSD using CNN model is higher than that of manual visual detection.

II. Method of RSD

II. A. Optical System Model

The optical model describes the process by which light reaches the image sensor from the LS through the surface of the object [11], [12]. Selecting the appropriate LS according to different detection objects is very important to optimize the mechanical surface detection effect. Rail surface defect detection is an important means to maintain railway safety. Due to the complex structure of rail surface, the forms of defects are diverse, and lighting conditions would affect the image quality and detection effect of rail surface.

The optical system model consists of LS, measured object and image sensor. The optical imaging model is displayed in Figure 1.

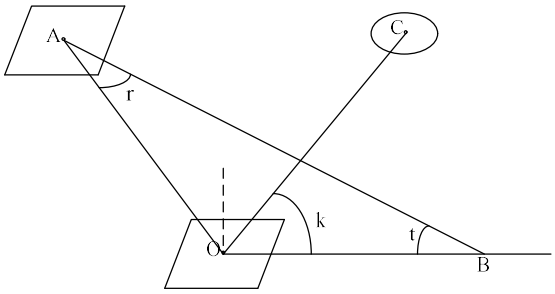

Figure 1: Optical imaging model

In Figure 1, an optical imaging model is depicted. In the machine vision system, the LS is usually used to irradiate the measured object, and then the industrial camera is used for image acquisition.

Let A be the LS point; O is the measured rail; C is the image sensor; point B is the intersection of the LS normal direction and the measured rail surface, and t represents the angle between the LS normal direction and the measured rail surface. r represents the angle between the direction of light emission and the normal direction of the LS, and k represents the angle between the axis center of the image sensor and the surface of the measured rail.

The GSV of the image of rail surface imaging is as follows:

$$M = G \cdot e \cdot U_1 \cdot U_2 \cdot U_3 \tag{1}$$

In Formula 1, G represents the scale coefficient; e represents the exposure time of the acquired image; U_1 represents the constant parameter; U_2 represents the illumination distance, camera equipment shooting distance and other parameters; U_3 represents the illumination angle and camera angle variables.

$$U_3 = {[-cos(t+k+r)] \cdot sin^2(r+t)}/{sin^2 t} \tag{2}$$

II. B.Rail Surface Image Acquisition

Because the longitudinal depth of the rail is much larger than the transverse depth, the linear CCD camera can capture high-resolution images when detecting rail surface defects. A strip LED LS is used as a lighting device, and a linear array CCD camera is selected for the camera, with a resolution of 4K.

The specifications of the rail are: rail head width: 70-150 mm, rail waist height: 130-200 mm, rail waist width: 130-150 mm, rail bottom width: 130-150 mm, and the line frequency of the camera is set to 17333HZ.

The rail surface image acquisition model is displayed in Figure 2.

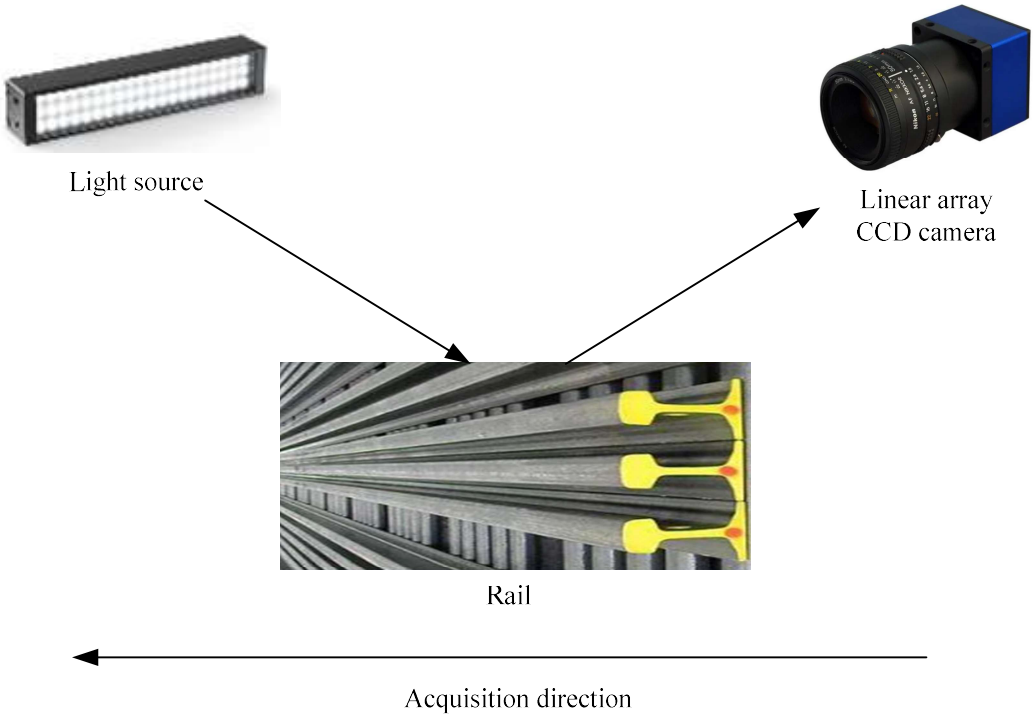

Figure 2: Model of rail surface image acquisition

In Figure 2, a rail surface image acquisition model is described. The direction of the acquisition system is from right to left. It should select the high-angle rail surface image to reduce the image misalignment caused by the vibration of the acquisition equipment.

When the rail surface image acquisition is carried out, it should control the relatively stable environment of the acquisition. To avoid direct sunlight, sunshade equipment can be used to reduce the interference of the environment on the rail surface image acquisition.

When the rail surface image is captured, the angle of the LS can be adjusted to better study the optical features of RSD. Table 1 displays the illumination characteristics of LS at various angles.

Table 1: Parameters of LS exposure at different angles

LS angle (°)	LS distance (mm)	Camera distance (mm)	Aperture number
15	280	360	2.8
30	280	360	2.8
45	280	360	2.8
60	280	360	2.8
75	280	360	2.8

In Table 1, the parameters under different LS conditions are described. In this text, 5 kinds of LS angles are set, and the LS distance, camera distance and aperture number are consistent.

The performance of RSD may also be related to the illumination color of the LS and the intensity of the LS. The LS color is adjusted by different LS and filters to set different LS environments, and the LS controller is used to adjust the intensity of the LS. The source colors set in this text are white, red, and blue, and the intensity of the LS ranges from 1000-10000 lumens.

There are 1000 images in the collected rail surface image data set, including 10 types of rail surface features. The rail surface image data set is displayed in Table 2.

Table 2: Image data set of rail surface

Serial number	Characteristic	Quantity	Proportion
1	Cracks	100	10.0%
2	Wear and tear	112	11.2%
3	Deformation	88	8.8%
4	Weld seam	106	10.6%
5	Rail bed damage	94	9.4%
6	Corrosion	112	11.2%
7	Welding defects	104	10.4%
8	Foreign object protrusion	106	10.6%
9	Normal	100	10.0%
10	Scratch	78	7.8%

In Table 2, the rail surface image dataset is described. The 10 types of rail surface images collected can effectively reflect the rail surface information.

The typical surface feature images in the collected rail surface images are displayed in Figure 3.

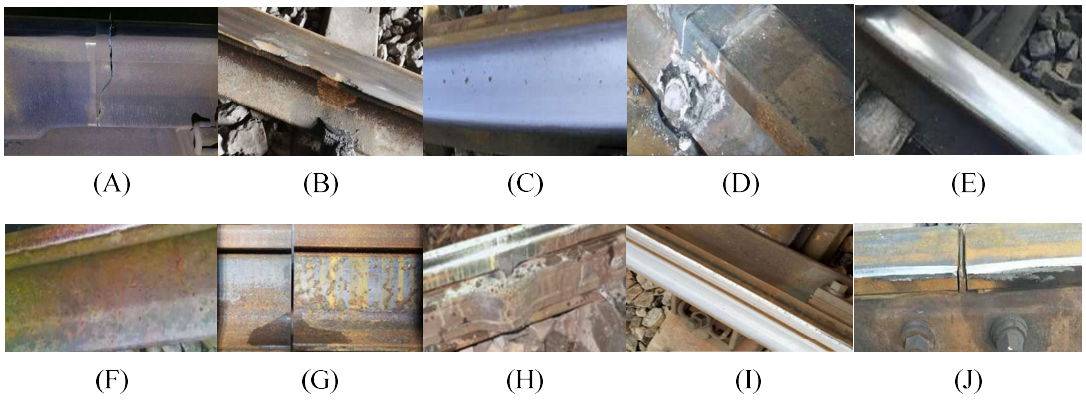

Figure 3: Image of rail surface

In Figure 3, the collected images of the rail surface are described. (A)~(J) respectively indicate crack, wear, deformation, weld, rail bed damage, corrosion, welding defect, foreign body protrusion, normal, scratch. Rail crack refers to the crack or crack defect in the steel railway track. Rail material fatigue and overloading are the main factors causing cracks. Rail cracks would reduce the strength and stability of rail, which is easy to cause railway transportation accidents.

The collected rail surface images were divided by Karpathy data set. Firstly, the collected images are manually labeled and described, and all the images in the data set are randomly scrambled to avoid potential correlation between the data. In this text, the scrambled data set is divided into 70% training, 15% data verification and 15% testing.

II. C.Image Preprocessing

In the process of rail surface image acquisition, due to the influence of linear array CCD camera equipment and external environmental factors, the rail surface image acquisition inevitably contains noise data. The noise data in the rail surface image would seriously interfere with the subsequent defect feature analysis, so it should preprocess the collected rail surface image.

The contents of image preprocessing include: image denoising and image enhancement, through which image quality can be improved and noise reduced [13], [14].

The essence of noise is the mutation of image GSV. In the process of image denoising, the collected rail surface image can be grayed first, and then the noise data can be eliminated by median filtering.

The formula for gray-scale image of rail surface is as follows:

$$Gray(i,j) = 0.299 \times R(i,j) + 0.587 \times G(i,j) + 0.114 \times B(i,j) \tag{3}$$

After grayscale processing of the original image, the median filter is used to filter out the noisy data [15], [16]. The formula of median filtering is expressed as:

$$\mathrm{y[n]} = \mathrm{median(x(n-k),\cdots,x[n],\cdots,x[n+k])} \tag{4}$$

The process of histogram equalization is as follows: firstly, the value of each pixel in the original rail surface image needs to be counted to obtain the original histogram, and then the original histogram needs to be cumulantly summed to map each pixel value to a new pixel value and replace the original pixel value to achieve image enhancement [17], [18]. The mapping process formula of pixels in histogram equalization is expressed as:

$$s = (L-1) * c(r)/(M*N) \tag{5}$$

In Formula 5, N represents the total number of pixel values; L represents the number of gray levels, and $c(r)$ represents the cumulative histogram.

The results of rail surface image preprocessing are displayed in Figure 4.

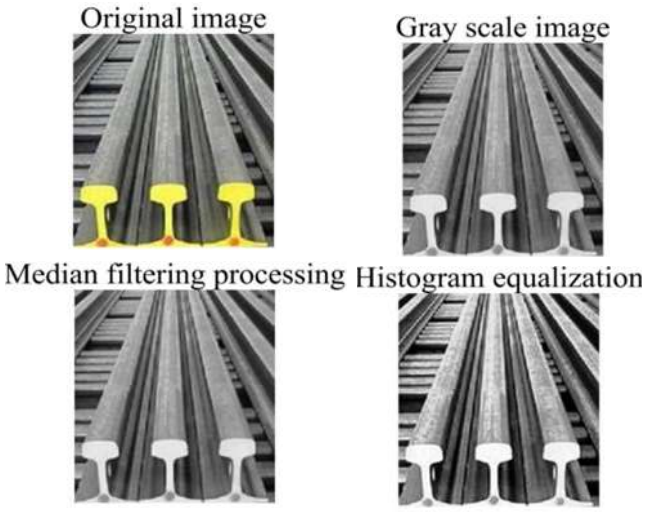

Figure 4: Results of rail surface image preprocessing

In Figure 4, the results of rail surface image preprocessing are described. After preprocessing the rail surface image, the noise data in the image can be well reduced and the image quality can be enhanced, which is beneficial to the subsequent feature extraction and feature detection analysis of the rail surface.

II. D.Image Feature Extraction

The extraction of surface features from the preprocessed rail images is helpful for the subsequent defect detection and classification analysis. Rail is an integral part of railway traffic. The goal of rail surface feature extraction is to inspect and assess rail surface defects, wear and corrosion.

In order to meet the needs of rail use, it should accurately classify the features of rail surface, and the extracted features need to have distinguishable characteristics. There are four main types of rail surface features, namely texture features, defect features, shape features and color features. Rail is a mechanical object, the surface of the inevitable appearance of various textures, such as scratches, friction and so on.

When texture features are extracted by gray co-occurrence matrix, contrast analysis can be used to reflect the depth of furrows in the image [19], [20]. The formula for using contrast to describe the difference degree of image gray level is expressed as:

$$\sum_{i,j} |i-j|^2 P(i,j) \tag{6}$$

In Formula 6, $P(i,j)$ represents the normalized gray co-occurrence matrix element.

The use of Canny edge detection algorithm to extract the edge information of the rail surface can effectively extract the defects that may exist on the rail surface, such as cracks, damage, wear, corrosion, etc., and extract the shape characteristics of the rail. The geometry of rail directly affects the safety of railway transportation. Canny edge detection algorithm can effectively detect the edge of the image when extracting defect features, which is usually the outline and shape information of the object in the rail image.

The color feature of rail surface is also an important discrimination index. By extracting the color feature of rail surface, it can detect the color change, color difference or stain and other defects of rail surface. The color moment can be used to extract the color features of the rail surface. By extracting the color features of the rail surface image, it can be used to identify the marks, stains or other surface defects of different colors.

The process of rail surface image feature extraction is displayed in Figure 5.

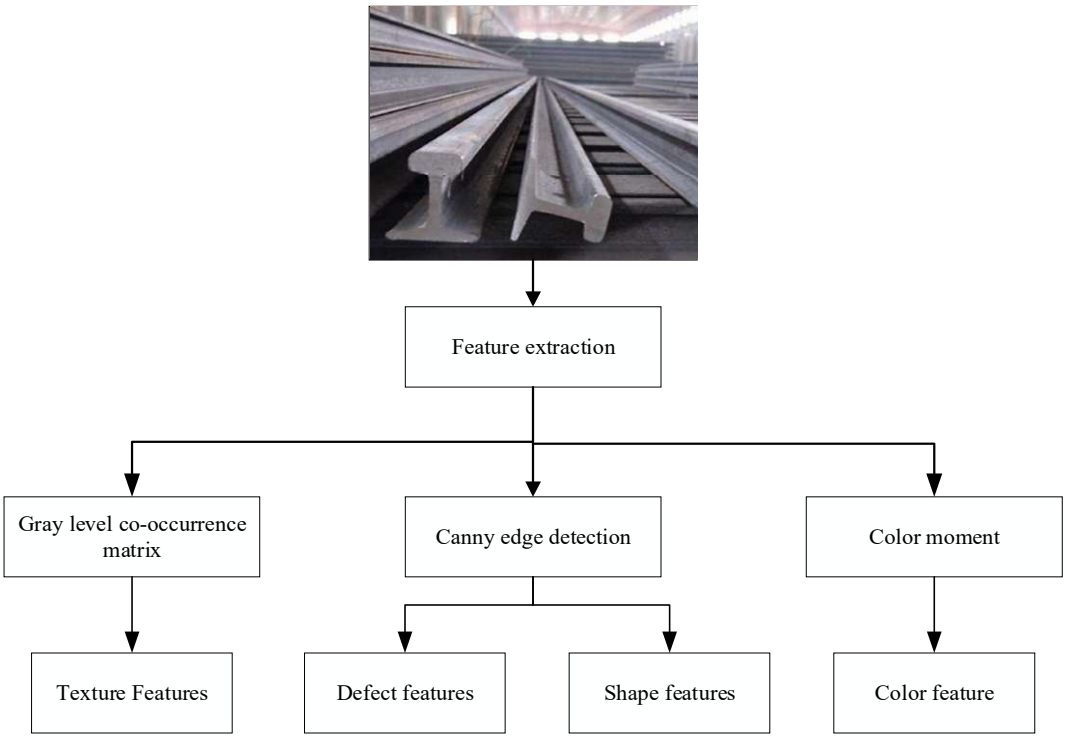

Figure 5: Feature extraction process of rail surface image

In Figure 5, the feature extraction process of rail surface image is described. In this text, the feature extraction of rail surface image is carried out in 4 directions.

II. E. RSD and Classification

Traditional machine vision methods need to manually design classifiers, while DL can handle large-scale data and complex tasks through automatic learning [21], [22].

CNN is a kind of neural network model which includes convolutional computation. It can learn local and global image features and accurately classify feature information [23], [24]. In this text, all kinds of images in the collected rail surface images are marked, so that each image has corresponding category label.

The steps of rail surface feature detection and classification using CNN are as follows: the preprocessed rail surface image is taken as input, and the convolution layer is used to extract the preliminary feature information from the rail surface image. The convolution kernel traverses all input images in a sliding form to obtain a two-dimensional convolution feature map. Finally, the classification of different rail surface types is realized through the fully connected layer.

The scale of the convolution kernel is smaller than the scale of the input image, and the single dimensions need to be consistent. In this text, the dimension of the input rail surface image is $5 \times 5 \times 1$, where 1 represents a single channel. Then the size of the convolution kernel can be set to $3 \times 3 \times 1$, and the dimension of the feature graph is expressed as:

$$K = {}^{N - m}/_{s} + 1 \tag{7}$$

In formula 7, N represents the input rail surface image scale; m represents the convolution kernel scale, and s represents the slide step size.

The feature map dimension of the convolution layer is very high. The pooling layer can reduce the feature map dimension by setting the pooling window and replacing the window feature with the most significant feature in the window. During the training of CNN model, the weight of convolutional kernel can be adjusted by error feedback analysis to achieve accurate classification of rail surface features. When the error reaches the acceptable range, it means that the CNN has completed the model training and can be used for the classification and analysis of rail surface features.

III. Rail Surface Inspection and Evaluation

Rail is an important part of railway traffic, and the surface safety detection of rail is very important for railway transportation [25], [26]. The defects existing on the rail surface would reduce the strength of the rail, which is easy to cause safety accidents. The optical model can realize non-contact high-precision surface inspection, and the application of machine vision optical model can effectively improve the efficiency of rail surface inspection.

III. A. Evaluation of Different Rail Surface Defects

The surface features of the rail are diversified, and the image GSVs corresponding to different surface features are different. In order to effectively analyze the image GSV corresponding to different surface feature information, this text analyzes rail cracks, rail wear, rail corrosion, welding defects, foreign body bumps, and normal rail. In order to analyze the change of GSV of image in defect area more accurately, this text takes rail crack image as an example to analyze. The environment under which the LS is set is as follows: white light irradiation, LS intensity is 5000 lumens, LS irradiation angle is 45°, and the defect depth of rail crack image is displayed in Table 3.

Table 3: Defect depth of rail crack image

Serial number	Crack depth (mm)	Number of images	Proportion
1	1	10	10.0%
2	2	8	8.0%
3	3	12	12.0%
4	4	13	13.0%
5	5	10	10.0%
6	6	7	7.0%
7	7	11	11.0%
8	8	11	11.0%
9	9	9	9.0%
10	10	9	9.0%

In Table 3, the defect depth of the rail crack image is described. In this text, a total of 10 kinds of surface crack depth images of rail are calculated. Rail crack depth refers to the depth of the rail surface or internal crack in the rail cross-section. The crack depth of the rail has an important effect on the safety, durability and running performance of the rail. When the crack depth of rail surface is large, the resistance of train running would be increased. When the surface crack depth of the rail is small, it is more difficult to detect and maintain the rail crack.

III. B. Change the Lighting Environment

In the image analysis of the rail surface, it is also necessary to analyze the different LS angles. When collecting the image data of the rail surface, this text obtains the images under 5 kinds of LS, which are 15°, 30°, 45°, 60° and 75° respectively. Taking the rail crack image as an example, the conditions for LS illumination are set as follows: white light irradiation, LS intensity of 5000 lumens, analysis of the overall GSV of the image under different LS irradiation angles under specific LS conditions and analysis of the difference between the GSV at the crack and the GSV of the surrounding normal rail.

III. C. Surface Inspection and Evaluation

After optical model analysis of rail surface images, this text selects CNN model to classify and predict rail surface features. In order to effectively analyze the feature classification effect of the optical model of RSD based on CNN model, it can be compared with the traditional manual visual detection method. The experiment also needs to compare and analyze the model studied in this text with other classical machine vision models. The classical Machine vision models were selected, including Support Vector Machine (SVM) and Random Forest (RF). The experiment was iterated 50 times to analyze the RSD effect of different models.

In order to evaluate the rail surface inspection effect of different models effectively, it should construct corresponding evaluation indexes. The classification of rail surface features is essentially a binary classification problem. The effect of rail surface classification is evaluated by statistical analysis of the actual classification results and the predicted classification results of rail surface images.

TP indicates that the prediction of rail surface classification is positive and the actual is also positive; FP indicates that the prediction of rail surface classification is positive but the actual is negative. FN means that the rail surface classification is predicted as a negative example but actually is a positive example; TN indicates that the rail surface classification was predicted to be negative and was actually negative.

Accuracy rate, recall rate, precision rate, F1 value, these four indexes reflect the classification effect of rail surface. The accuracy is expressed as:

$$A = {(TP + TN)}/{N} \tag{8}$$

In Formula 8, N represents the total number of samples of rail surface images.

The formula of precision rate is expressed as:

$$P = {TP}/{(TP + FP)} \tag{9}$$

$$R = {TP}/{(TP + FN)} \tag{10}$$

F1 value is expressed as:

$$F1 = {2(P \times R)}/{(P + R)} \tag{11}$$

By counting the actual and predicted results of rail surface characteristics, Receiver Operating Characteristic (ROC) curve can be drawn, and the classification effect of rail surface can be directly reflected by the ROC curve.

IV. Results

IV. A. GSV of Image of Different Rail Surface Defects

In the process of production, due to improper heat treatment, uneven metal materials and other reasons, the surface of the rail presents different defect characteristics. In this text, the GSV information of 6 kinds of rail surface images including rail crack, rail wear, rail corrosion, welding defect, foreign body protrusion and normal rail are counted. The GSV results of images of different rail surfaces are displayed in Figure 6.

In Figure 6, the image GSV results of different rail surfaces are described. The GSV range of the rail surface image is between [0,255], and the higher the GSV, the brighter the image.

The normal rail surface is usually smooth, metallic, and its surface reflects more light. Normal rail surface images may appear as brighter areas, corresponding to higher GSVs. Defects in the rail surface would reduce the reflected light, which would appear as darker areas in the image. The GSV of the foreign body convex image is higher than that of the rail concave image. This is mainly due to the concave part of the rail may cause dark spots in the image, making the GSV low.

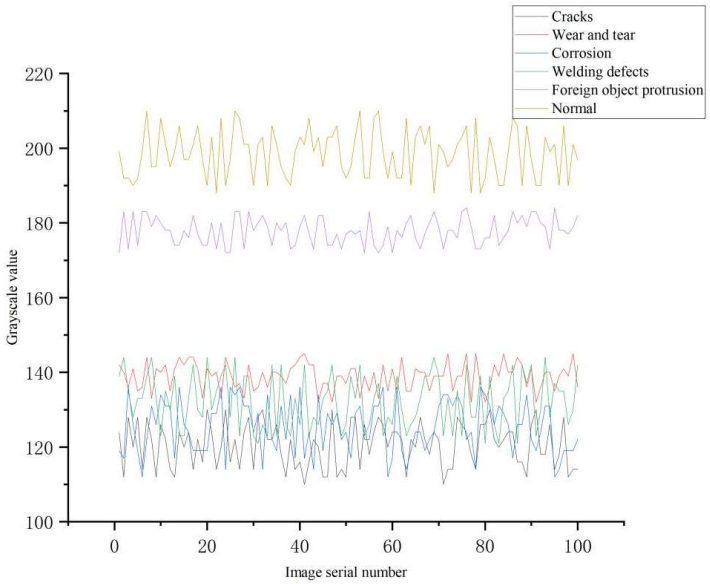

Figure 6: GSV results of images of different rail surface defects

IV. B. Results of Rail Surface Crack Depth

Rail cracks are a common surface feature. Cracks of different depths were selected for analysis in the experiment. The comparison results of GSVs of cracks of different rail surface depths are displayed in Figure 7.

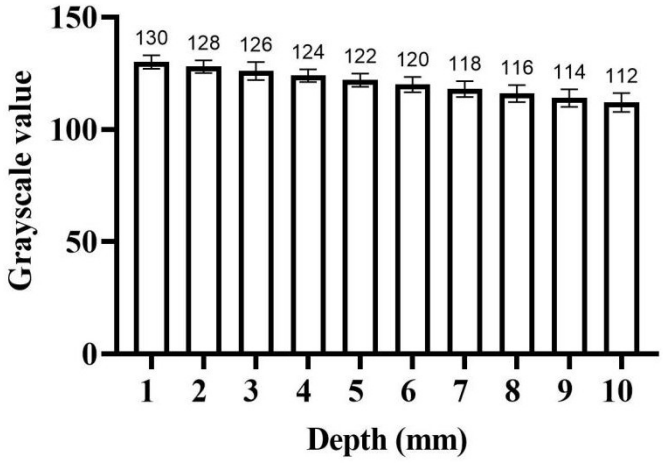

Figure 7: GSV of crack depth on different rail surfaces

In Figure 7, the GSVs of crack depths on different rail surfaces are described. The horizontal axis indicates the depth of cracks on the rail surface, and the depth of cracks is between 1-10mm. The GSV of rail crack surface image decreases with the increase of crack depth. The average GSV of the image was 130 when the rail surface crack depth was 1mm, and 112 when the rail surface crack depth was 10mm.

The deeper the crack of the rail, then the crack defect would cause serious light scattering, reflection or absorption, resulting in lower brightness at the crack defect. Therefore, the depth, size and location of defects can be evaluated quantitatively by analyzing the GSV change of the defect area.

IV. C. Result of LS Irradiation Angle

The illumination angle of the LS is also the main reason that affects the GSV of the rail surface image. The illumination angles of LS set in this text are respectively 15°, 30°, 45°, 60° and 75°. The GSVs of rail crack images under different illumination angles are displayed in Figure 8.

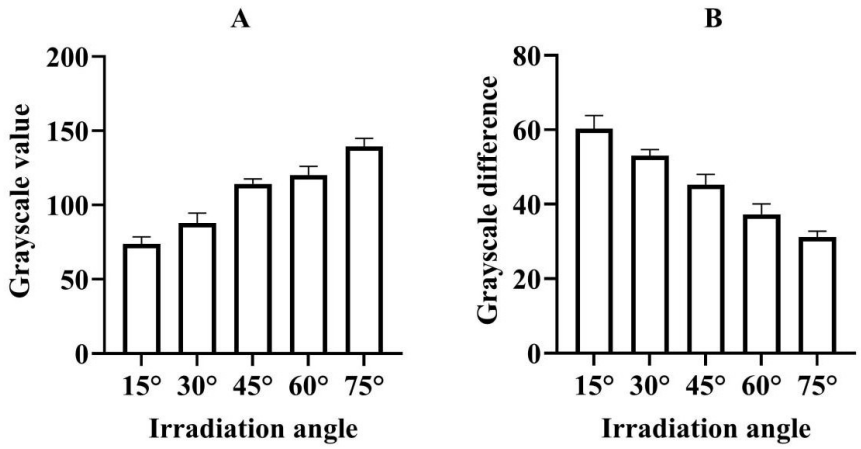

Figure 8: GSVs under different LS irradiation angles

Figure 8(A) overall GSV

Figure 8(B) The difference between the GSV at the crack and that of the normal rail

In Figure 8(A), the overall GSV of the rail crack image is described. The horizontal axis denotes the irradiation angle conditions of different LS, and the vertical axis denotes the overall GSV of the rail crack image. The smaller the irradiation angle of LS, the smaller the overall GSV of the rail crack image. This is mainly due to the smaller the angle between the direction of the LS and the rail, resulting in a smaller reflection of the light into the camera, which leads to a reduction in the overall GSV.

Figure 8(B) describes the difference between the GSV at the crack and the GSV of the normal rail. The horizontal axis represents the irradiation angle of different LS, and the vertical axis represents the gray difference. The smaller the illumination angle of the LS, the greater the difference between the GSV at the crack and the normal rail GSV. LS irradiation angle is small line LS irradiation would produce strong shadow effect, so that the crack in the image is relatively dark, and the GSV of the surrounding normal rail is much different. In this case, the cracks are easily highlighted, which is conducive to the identification of defects. However, when the illumination angle of the LS is large, the brightness value of the cracked part would be close to the surrounding normal rail, resulting in the GSV of the cracked area and the normal rail area.

The images of rail cracks under different LS irradiation angles are displayed in Figure 9.

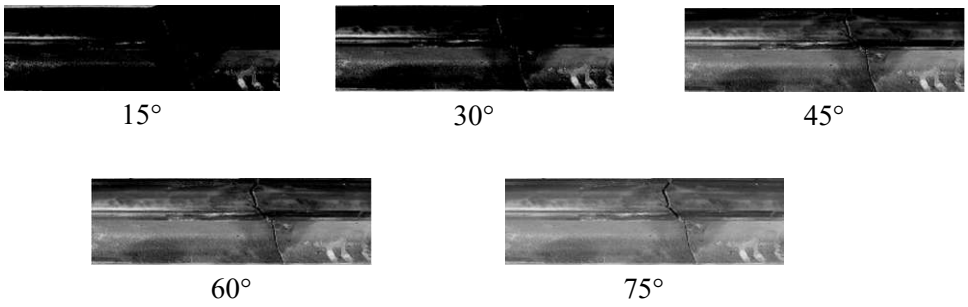

Figure 9: Images of rail cracks under different LS irradiation angles

In Figure 9, the image of rail crack under different LS irradiation angles is described. The smaller the angle of the LS, the darker the overall image; the larger the angle of the LS, the brighter the overall image.

In this text, the CNN is used to detect the rail surface under different LS angles, and the accuracy of RSD features under different LS angles is calculated. The accuracy results of RSD under different LS angles are displayed in Figure 10.

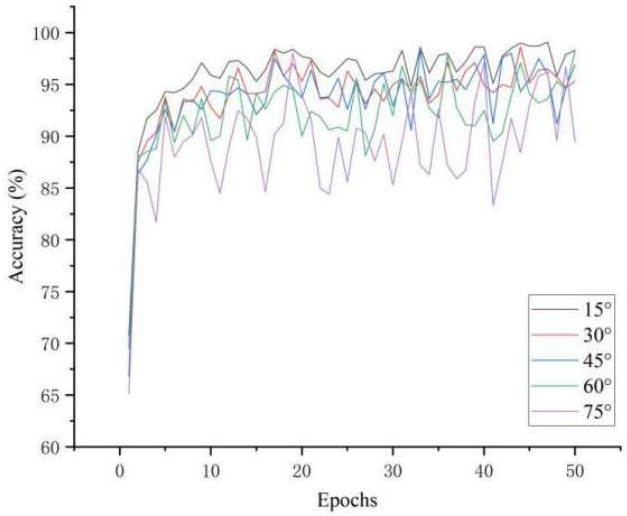

Figure 10: RSD accuracy under different LS angles

In Figure 10, the accuracy of RSD under different LS angles is described. The horizontal axis represents the training period of the CNN model, and the vertical axis represents the detection accuracy of rail surface features. It was obvious that the feature detection accuracy of the CNN model was the highest when the LS angle was 15°. With the increase of the illumination angle of the LS, the accuracy of the CNN for RSD decreases. When Epochs was 50, the accuracy of RSD was 98.3%, 95.3%, 96.9%, 98.2% and 89.5% for 15°, 30°, 45°, 60° and 75° illumination angles, respectively.

Under the smaller LS irradiation angle, the influence of light reflection can be effectively reduced, so as to better expose the rail surface characteristics, which can improve the accuracy of RSD.

IV. D. Results of LS Color

Different LS colors have different spectral distribution, and the change of LS colors would affect the color information in optical images. The GSV results of images irradiated by white light, red light and blue light are displayed in Figure 11.

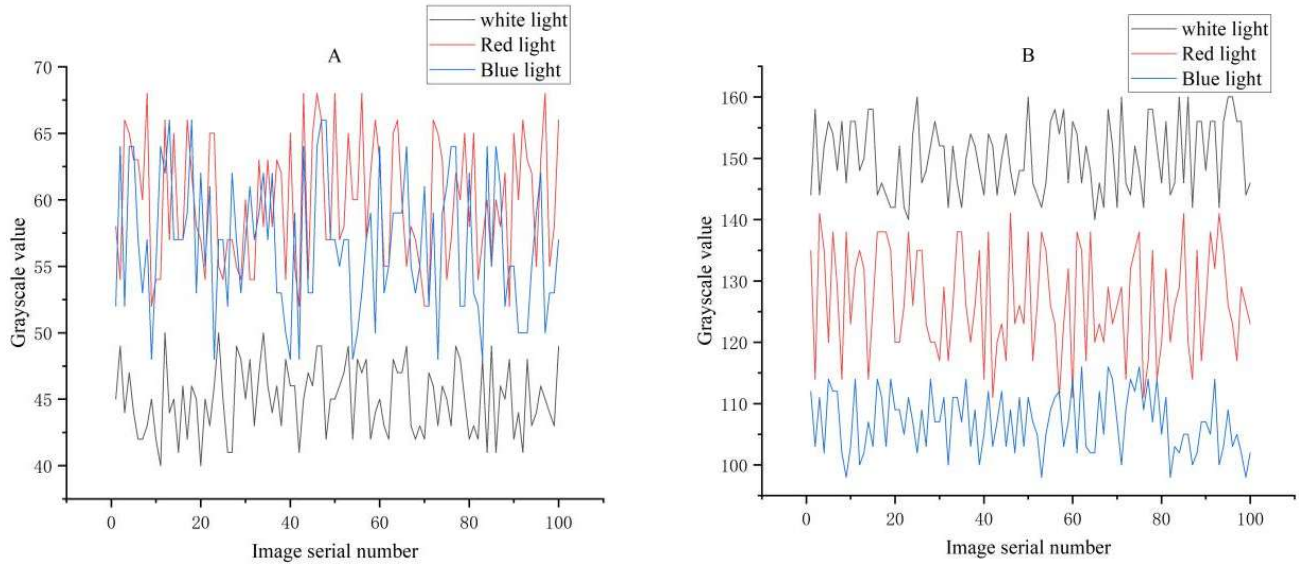

(A) GSV at the crack (B) GSV of non-crack area

Figure 11: Color analysis results of LS

Figure 11(A) describes the GSV at the crack under the irradiation of three different LS colors. The GSV at the crack under the irradiation of white light is the lowest, while the GSV at the crack under the irradiation of blue light and red light is not much different.

By analyzing the GSVs of cracks and non-cracks under different LS colors, the GSVs of images can be the most different under white light irradiation, which is helpful for RSD. White light encompasses the entire visible spectrum and provides comprehensive surface information.

IV. E. Result of LS Intensity

The intensity of the LS is governed by the LS controller. The intensity range of the LS is set at an illumination angle of 15° and the colour of the LS is white. The analysis results of the intensity of different LS are displayed in Figure 12.

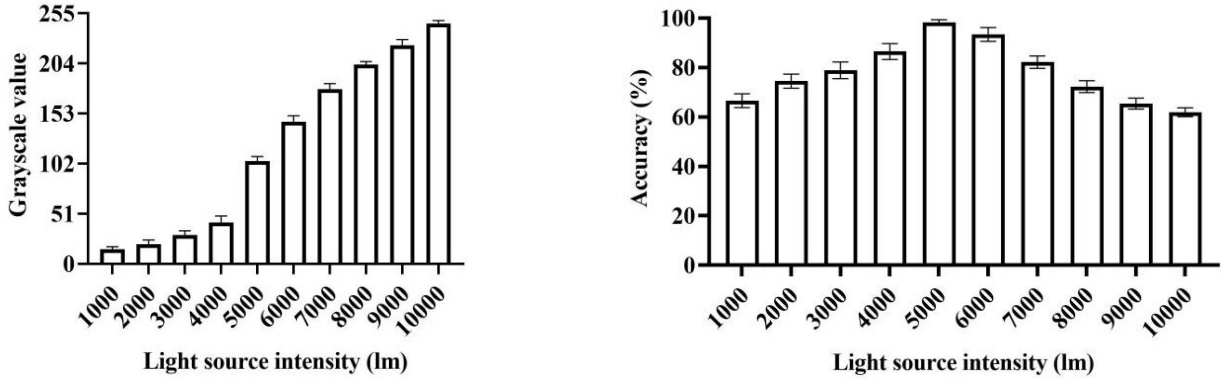

(A) GSVof crack image (B) Crack detection accuracy

Figure 12: Analysis results of different LS intensities

In Figure 12(A), GSVs of crack images under different LS intensities are described, and the LS intensities range from 1000 lumens to 10,000 lumens. When the LS intensity was between [1000 and 4000], the GSV of the image of the rail crack surface was relatively low. The higher the LS intensity is, the higher the GSV of the image is. The LS intensity is too high or too low would cause the image of rail crack surface to appear over exposure or low brightness phenomenon. When the LS intensity was 5000 lumens, the GSV range of the image was appropriate, and the details can be clearly visible.

In Figure 12(B), the accuracy of crack detection under different LS is described. The horizontal axis represents different LS intensity ranges, and the vertical axis represents average crack detection accuracy. The average crack detection accurately increased first and then decreased. When the LS intensity was 5000 lumens, the crack detection accuracy reached the highest, and the average crack detection accuracy was 98.2%. When the LS intensity is too high, it causes the brightness value to exceed the dynamic range of the sensor or camera, resulting in loss of detail and areas becoming too bright. When the intensity of the LS is too low, the brightness value is too low, and the details are submerged in the darkness, making it difficult to perform accurate feature detection. Controlling the LS in the appropriate intensity range can effectively improve the accuracy of rail surface image detection.

IV. F. RSD Accuracy of Different Models

The illumination angle of the LS set in this text is 15°. The LS color is white and the LS intensity is 5000 lumens. In this text, the CNN model is compared with a variety of rail surface inspection models. The traditional rail surface inspection uses manual visual inspection. The accuracy results of RSD of different models are displayed in Figure 13.

In Figure 13, the accuracy of RSD of different models is described, while the accuracy of traditional manual visual detection has little difference in 50 tests. The accuracy of RSD based on CNN model is higher than that of SVM and RF model. With Epochs 50, the accuracy of RSD by CNN model, SVM, RF and traditional manual visual detection was 98.3%, 93.8%, 89.4% and 77.5%, respectively.

The CNN model has excellent automatic feature learning ability, and can accurately extract and detect the complex texture, shape and structure feature information of the rail surface. The traditional manual visual inspection is greatly affected by manual experience and easy to be interfered by external environmental factors. SVM and RF model are difficult to process the global rail surface features.

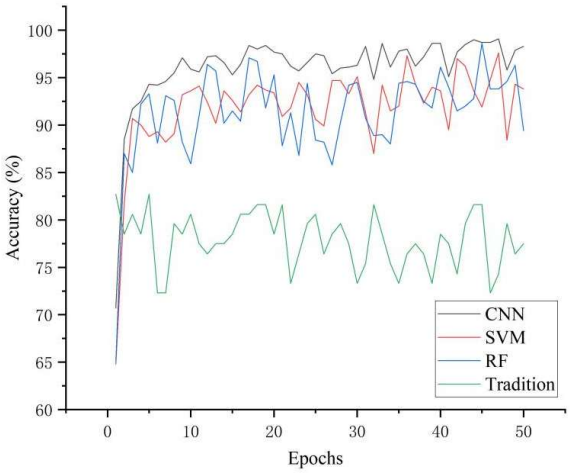

Figure 13: RSD accuracy of different models

In order to more intuitively analyze the effect of different models on rail surface feature detection, ROC curve images of CNN model, SVM and RF were drawn in this text. The ROC curve image is displayed in Figure 14.

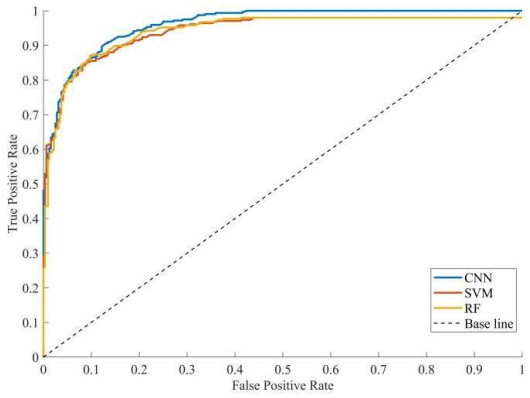

Figure 14: Image of ROC curve

In Figure 14, the ROC curve of rail surface feature detection under different machine vision models is described. The line between point (0,0) and point (1,1) is the base line. The points on the baseline indicate that the true case rate is equal to the false positive case rate, indicating that the model is a completely random prediction model. The curve based on the CNN model is closer to the point (0,1), which means that the accuracy rate of the CNN model is higher, and the area under the curve of the CNN model is the largest. The application of CNN model to RSD can effectively improve the accuracy of surface feature detection.

V. Conclusions

Rail is the foundation of railway transportation, and its safety condition directly affects the safety of train running. In this text, the linear array CCD camera is used to collect a large number of rail images, and the optical system model is established. The rail surface features are detected by preprocessing the rail surface images and training the model. The detection effect of rail surface features is related to the given lighting conditions. The optical characteristics of rail surface are analyzed by adjusting the incidence angle of light, setting the color of LS and adjusting the intensity of LS. The experimental results show that the GSV of the foreign body convex image is higher than that of the rail concave image, and the deeper the crack depth of the rail surface, the darker the image. The smaller the illumination angle of the LS, the lower the overall GSV, but the greater the difference between the GSV at the crack and the normal rail GSV. The GSV of the image can be the most different under white light irradiation, which is helpful for RSD. In this text, the accuracy of RSD using CNN model is better than that of manual visual detection, SVM and RF model. However, this text lacked specific optical characteristics analysis of different rail surface characteristics, so the optical characteristics analysis of different rail surface characteristics can be the direction of future research.

Funding

This work was supported by the National Natural Science Foundation of Shandong (Grant No. ZR2019MEEO59).

References

[1] Mohan, Arun, and Sumathi Poobal. "Crack detection using image processing: A critical review and analysis." alexandria engineering journal 57.2 (2018): 787-798.
[2] Borwankar, Raunak, and Reinhold Ludwig. "An optical surface inspection and automatic classification technique using the rotated wavelet transform." IEEE Transactions on Instrumentation and Measurement 67.3 (2018): 690-697.
[3] Xu, Xiangyang, Hao Yang, Riccardo Augello & Erasmo Carrera. "Optimized free-form surface modeling of point clouds from laser-based measurement." Mechanics of Advanced Materials and Structures 28.15 (2021): 1570-1578.
[4] Mei, Shuang, Hua Yang, and Zhouping Yin. "An unsupervised-learning-based approach for automated defect inspection on textured surfaces." IEEE Transactions on Instrumentation and Measurement 67.6 (2018): 1266-1277.
[5] Ahmed, Junaid, Bin Gao, and Wai Lok Woo. "Wavelet-integrated alternating sparse dictionary matrix decomposition in thermal imaging CFRP defect detection." IEEE Transactions on Industrial Informatics 15.7 (2018): 4033-4043.
[6] Sirca Jr, Gene F., and Hojjat Adeli. "Infrared thermography for detecting defects in concrete structures." Journal of Civil Engineering and Management 24.7 (2018): 508-515.
[7] Luo, Qiwu, Xiaoxin Fang, Li Liu, Chunhua Yang, Yichuang Sun. "Automated visual defect detection for flat steel surface: A survey." IEEE Transactions on Instrumentation and Measurement 69.3 (2020): 626-644.
[8] Baumgartl, Hermann, Josef Tomas, Ricardo Buettner & Markus Merkel. "A deep learning-based model for defect detection in laser-powder bed fusion using in-situ thermographic monitoring." Progress in Additive Manufacturing 5.3 (2020): 277-285.
[9] Goh, Guo Dong, Nur Muizzu Bin Hamzah, and Wai Yee Yeong. "Anomaly detection in fused filament fabrication using machine learning." 3D Printing and Additive Manufacturing 10.3 (2023): 428-437.
[10] Min, Yongzhi, Benyu Xiao, Jianwu Dang, Biao Yue & Tiandong Cheng. "Real time detection system for rail surface defects based on machine vision." EURASIP Journal on Image and Video Processing 2018.1 (2018): 1-11.
[11] Buscombe, Daniel. "SediNet: A configurable deep learning model for mixed qualitative and quantitative optical granulometry." Earth Surface Processes and Landforms 45.3 (2020): 638-651.
[12] Sitzmann, Vincent, Steven Diamond, Yifan Peng, Xiong Dun, Stephen Boyd, Wolfgang Heidrich, et al. "End-to-end optimization of optics and image processing for achromatic extended depth of field and super-resolution imaging." ACM Transactions on Graphics (TOG) 37.4 (2018): 1-13.
[13] Moradmand, Hajar, Seyed Mahmoud Reza Aghamiri, and Reza Ghaderi. "Impact of image preprocessing methods on reproducibility of radiomic features in multimodal magnetic resonance imaging in glioblastoma." Journal of applied clinical medical physics 21.1 (2020): 179-190.
[14] Ranganathan, Dr G. "A study to find facts behind preprocessing on deep learning algorithms." Journal of Innovative Image Processing 3.1 (2021): 66-74.
[15] Bayar, Belhassen, and Matthew C. Stamm. "Constrained convolutional neural networks: A new approach towards general purpose image manipulation detection." IEEE Transactions on Information Forensics and Security 13.11 (2018): 2691-2706.
[16] Mafi, Mehdi, Hoda Rajaei, Mercedes Cabrerizo, Malek Adjouadi. "A robust edge detection approach in the presence of high impulse noise intensity through switching adaptive median and fixed weighted mean filtering." IEEE Transactions on Image Processing 27.11 (2018): 5475-5490.
[17] Agrawal, Sanjay, Rutuparna Panda, P.K. Mishro, Ajith Abraham. "A novel joint histogram equalization based image contrast enhancement." Journal of King Saud University-Computer and Information Sciences 34.4 (2022): 1172-1182.
[18] Vijayalakshmi, D., and Malaya Kumar Nath. "A novel contrast enhancement technique using gradient-based joint histogram equalization." Circuits, Systems, and Signal Processing 40.8 (2021): 3929-3967.
[19] Khaldi, Belal, Oussama Aiadi, and Mohammed Lamine Kherfi. "Combining colour and grey-level co-occurrence matrix features: a comparative study." IET Image Processing 13.9 (2019): 1401-1410.
[20] Kaya, Yılmaz, Melih Kuncan, Kaplan Kaplan, Mehmet Recep Minaz. "A new feature extraction approach based on one dimensional gray level co-occurrence matrices for bearing fault classification." Journal of Experimental & Theoretical Artificial Intelligence 33.1 (2021): 161-178.
[21] Ghosal, Sambuddha, David Blystone, Asheesh K. Singh and Soumik Sarkar. "An explainable deep machine vision framework for plant stress phenotyping." Proceedings of the National Academy of Sciences 115.18 (2018): 4613-4618.
[22] Singh, Swarit Anand, and K. A. Desai. "Automated surface defect detection framework using machine vision and convolutional neural networks." Journal of Intelligent Manufacturing 34.4 (2023): 1995-2011.
[23] Ghazal, T. M. "Convolutional neural network based intelligent handwritten document recognition." Computers, Materials & Continua 70.3 (2022): 4563-4581.
[24] Sharma, Tripti, Rajit Nair, and S. Gomathi. "Breast cancer image classification using transfer learning and convolutional neural network." International Journal of Modern Research 2.1 (2022): 8-16.
[25] Gan, Jinrui, Jianzhu Wang, Haomin Yu, Qingyong Li, Zhiping Shi. "Online rail surface inspection utilizing spatial consistency and continuity." IEEE Transactions on Systems, Man, and Cybernetics: Systems 50.7 (2018): 2741-2751.
[26] Wu, Yunpeng, Yong Qin, Yu Qian, Feng Guo, Zhipeng Wang, Limin Jia, et al. "Hybrid deep learning architecture for rail surface segmentation and surface defect detection." Computer-Aided Civil and Infrastructure Engineering 37.2 (2022): 227-244.